# Thermodynamic evolution of cosmological baryonic gas. I. Influence of non-equipartition processes

S. Courty, Jean-Michel Alimi

A&A 416, 875–888 (2004)
DOI: 10.1051/0004-6361:20031736


Astronomy & Astrophysics

# Thermodynamic evolution of cosmological baryonic gas

## I. Influence of non-equipartition processes

S. Courty[1,2] and J. M. Alimi[1]

[1] Laboratoire de l'Univers et de ses Théories, CNRS UMR 8102, Observatoire de Paris-Meudon, 5 place Jules Janssen, 92195 Meudon Cedex, France
e-mail: jean-michel.alimi@obspm.fr
[2] Present address: Science Institute, University of Iceland, Dunhagi 3, 107 Reykjavik, Iceland

Received 6 March 2003 / Accepted 11 December 2003

**Abstract.** Using N-body/hydrodynamic simulations, the influence of non-equipartition processes on the thermal and dynamical properties of cosmological baryonic gas is investigated. We focus on a possible departure from equilibrium between electrons, ions and neutral atoms in low temperature ($10^4$–$10^6$ K) and weakly ionized regions of the intergalactic medium. The simulations compute the energy exchanges between ions, neutrals and electrons, without assuming thermal equilibrium. They include gravitation, shock heating and cooling processes, and follow self-consistently the chemical evolution of a primordial composition hydrogen-helium plasma without assuming collisional ionization equilibrium. At high redshift, a significant fraction of the intergalactic medium is found to be warmer and weakly ionized in simulations with non-equipartition processes than in simulations in which the cosmological plasma is considered to be in thermodynamic equilibrium. With a semi-analytical study of the out of equilibrium regions we show that, during the formation of cosmic structures, departure from equilibrium in accreted plasma results from the competition between the atomic cooling processes and the elastic processes between heavy particles and electrons. Our numerical results are in agreement with this semi-analytical model. Therefore, since baryonic matter with temperatures around $10^4$ K is a reservoir for galaxy formation, non-equipartition processes are expected to modify the properties of the objects formed.

**Key words.** cosmology: theory – cosmology: large-scale structure of the universe – galaxies: intergalactic medium – galaxies: formation – hydrodynamics

## 1. Introduction

In the basic picture of galaxy formation, baryons fall into dark matter potential wells located along the network of sheets and filaments formed by gravitational instability (Sunyaev & Zel'dovich 1972; Rees & Ostriker 1977; Silk 1977; White & Rees 1978). In this hierarchical picture, galaxy clusters result from the large scale collapse of gas and from mergers of subunits. These massive structures ($M > 10^{14}\ M_\odot$) are mainly present at low redshift ($z < 2$). Mergers and accretion of matter involve hydrodynamical shocks raising the intracluster medium temperature to more than $10^7$ K. On the other hand in galaxy-size structures, shocks and gravitational compression do not heat the intergalactic medium to such high temperatures and the gas can cool to a few times $10^4$ K and concentrate to form galaxies. The intergalactic medium (IGM) refers to the cosmological gas in gravitationally bound structures[1]. The hierarchical scenario causes the IGM to separate into two phases: the hot intra-cluster medium at $T > 10^6$ K and the cold intergalactic medium at a few times $10^4$ K (Cen et al. 1993; Evrard et al. 1994). But the process of accretion and cooling of baryons inside bounded structures is still not well understood and a study of the thermodynamic properties of the IGM is crucial to our understanding of galaxy formation.

The cosmological plasma accreted in bound structures acquires thermal energy through gravitational compression and shock heating. The increase in temperature heats preferentially heavy particles and owing to the large difference in mass between heavy particles and electrons the energy transfer between both species is poorly efficient (Zel'dovich & Raizer 1966). The outer regions of bound structures then consist of a non-equilibrium two temperature gas. In this paper we introduce non-equipartition processes between ions, neutrals and

*Send offprint requests to*: S. Courty,
e-mail: courty@raunvis.hi.is

[1] In large scale structure formation simulations, the word structure refers to any potential well created by the dark matter. This sense is then more general than referring only to galaxies, since in such potential wells a number of galaxies can form. Hence the cosmological gas in gravitationally bound structures, the medium inside potential wells, is often referred to as intergalactic medium in the literature (Cen & Ostriker 1993; Davé et al. 2001).

electrons of the cosmological plasma in numerical simulations of large scale structure formation in order to investigate their influence on the thermodynamic properties of baryons. The results are compared to simulations in which equipartition processes are forced. The simulations are performed with an Eulerian N-Body/hydrodynamical code including gravitation, shock heating and radiative cooling processes.

Depending on the depth of the potential wells, the temperature of the accreted baryonic matter ranges from $10^4$ to $10^8$ K. At high temperatures, the accreted matter is totally ionized behind shock fronts and departure from equilibrium between ions and electrons is due to the quite long energy exchange timescale between these species. The thermal decoupling between ions and electrons in galaxy clusters has been considered by several authors (Fox & Loeb 1997; Chièze et al. 1998; Takizawa & Mineshige 1998; Takizawa 1998). Indeed Chièze et al. (1998) show that temperatures of these two species can be significantly different, by a factor of ∼3, in the outer regions of galaxy clusters. Our large scale simulations do show such temperature differences in massive structures at low redshift.

The simulations also show departure from equilibrium in structures much less massive than galaxy clusters. These structures are characterized by a warm plasma with heavy particle temperature between $10^4$ and $10^6$ K and electron temperature at a few times $10^4$ K. That plasma is also weakly ionized. We show that the fraction of warm IGM dramatically increases at high redshift because of the larger number of low mass structures, formed in hierarchical models. Departure from equilibrium is not only due to Coulomb interactions between charged particles, but also due to mechanisms of short-range forces between electrons and neutral particles (Petschek & Byron 1957; Shchekinov 1991). In such low density IGM, equilibration timescales between these species are short compared to the Hubble time and we propose a semi-analytical model to explain them. This model suggests some insights into the thermodynamical story of cosmological baryonic gas.

In this paper we focus on the low mass structure case and examine in detail the thermodynamic properties of the baryons. We show how non-equipartition processes, inside bound structures, at high redshift and before the reionization epoch, yields a large fraction of the IGM to be warm (between $10^4$–$10^6$ K) and we discuss the implications for galaxy formation. The paper is organized as follows. Section 2 presents the numerical code and simulations. In Sect. 3 influence of non-equipartition processes on the thermodynamic properties of baryons are analyzed. Section 4 gives, with the aid of a semi-analytical model, the physical origin of departure from equilibrium in the low mass structure case. Finally Sect. 5 discusses the cosmological implications for galaxy formation.

## 2. Simulations

Simulations are performed with a 3 dimensional N-body/hydrodynamical code coupling a Particle-Mesh code to compute gravitational forces with an Eulerian (pseudo-Lagrangian) hydrodynamical code (Teyssier et al. 1998). The gravitational potential is solved from the dark matter and the gas density fields. The main feature of the code is the computation of non-equipartition processes between ions, neutrals and electrons. Each species of the cosmological plasma has its own specific internal energy, $e_\mathrm{i}$, $e_\mathrm{n}$, $e_\mathrm{e}$, satisfying the energy conservation equation:

$$\left(\rho\frac{\mathrm{D}e}{\mathrm{D}t} = -p(\boldsymbol{\nabla}\cdot v) + \Psi - \Lambda_\mathrm{net}\right)_x, \tag{1}$$

where $\rho_x$ is the density, $e_x$ the specific internal energy, $p_x = n_x k T_x$ the partial pressure and $n_x$ the number density for the $x$ species. We do not distinguish the velocity $v$ for the three species. $\Psi$ is a dissipative term due to shock heating and $\Lambda_\mathrm{net}$ is a net cooling term containing the radiative cooling rates (heating and cooling processes) and the energy exchange rates between species. We now briefly discuss the two terms of the energy equation, shock heating and elastic or inelastic processes, computed separately in the code.

Shock heating is treated using the artificial viscosity method (Von Neumann & Richtmyer 1950). To reduce numerical dissipation, the contribution of shocks to the energy is computed from a pseudo-entropy equation:

$$\left(\frac{\mathrm{D}s}{\mathrm{D}t} = \frac{s}{e}V_\mathrm{s}\Psi\right)_x, \tag{2}$$

where the pseudo-entropy $s_x$ for the species $x$ is defined by $e_x V_\mathrm{s}^{\gamma-1}$ with gamma being the ratio of specific heats and $V_\mathrm{s}$ the specific volume. The viscous dissipation function is:

$$\Psi = -Q_\mathrm{v}(\boldsymbol{\nabla}\cdot v), \tag{3}$$

where the term $Q_\mathrm{v}$ equals $-p(C_1\varepsilon + C_2\varepsilon^2)$ with $\varepsilon = \Delta x\boldsymbol{\nabla}\cdot v/c_\mathrm{s}$. $\Delta x$ is the physical length of the cell and $c_\mathrm{s}$ the sound velocity. The constants $C_1$ and $C_2$ are determined experimentally and set to 1 in the simulations (the sensitivity to these constants are discussed in Sect. 3.3). The advantage of solving an equation for the pseudo-entropy rather than the internal energy is that an adiabatic flow remains strictly adiabatic.

The net cooling term is expressed as the contribution of three terms:

$$\Lambda_\mathrm{net} = \mathcal{H} + \Lambda + Q_\mathrm{exch}, \tag{4}$$

where $\mathcal{H}$ is a heating term for example due to photoionization processes (see Sect. 5), $\Lambda$ is the sum of the cooling rates and $Q_\mathrm{exch}$ denotes the energy exchange between interacting species.

Radiative cooling processes considered here are: collisional excitation, collisional ionization, recombination, bremsstrahlung and Compton scattering. Ionization and heat input from the ultraviolet radiation background are not included (this point is discussed in Sect. 5). The computation of cooling rates needs to follow the chemical evolution of a primordial composition hydrogen-helium plasma with $n_\mathrm{H}$ and $n_\mathrm{He}$ the number densities of hydrogen and helium, respectively. It must be noted that collisional ionization equilibrium is not assumed here. The density evolution for the six species of the plasma ($\mathrm{H}^0$, $\mathrm{He}^0$, $\mathrm{H}^+$, $\mathrm{He}^+$, $\mathrm{He}^{++}$, e) are solved with:

$$-\beta_{\mathrm{H}^0} n_\mathrm{e} n_{\mathrm{H}^0} + \alpha_{\mathrm{H}^+} n_\mathrm{e} n_{\mathrm{H}^+} = \frac{\partial n_{\mathrm{H}^0}}{\partial t}, \tag{5}$$

$$-\beta_{\mathrm{He}^0} n_\mathrm{e} n_{\mathrm{He}^0} + \alpha_{\mathrm{He}^+} n_\mathrm{e} n_{\mathrm{He}^+} = \frac{\partial n_{\mathrm{He}^0}}{\partial t}, \tag{6}$$

$$\beta_{\mathrm{He}^+} n_\mathrm{e} n_{\mathrm{He}^+} - \alpha_{\mathrm{He}^{++}} n_\mathrm{e} n_{\mathrm{He}^{++}} = \frac{\partial n_{\mathrm{He}^{++}}}{\partial t}, \tag{7}$$

**Table 1.** Ionization and recombination rates expressed in $s^{-1}$ $cm^3$ (from Black 1981 and Cen 1992) with $T_{en} = T_e/10^n$ K the electron temperature.

| Ionization rates: |
|---|
| $\beta_{H^0} = 5.85 \times 10^{-11}(1 + T_{e5}^{1/2})^{-1} e^{(-157809.1/T_e)} T_e^{1/2}$ |
| $\beta_{He^0} = 2.38 \times 10^{-11}(1 + T_{e5}^{1/2})^{-1} e^{(-285335.4/T_e)} T_e^{1/2}$ |
| $\beta_{He^+} = 5.68 \times 10^{-12}(1 + T_{e5}^{1/2})^{-1} e^{(-631515/T_e)} T_e^{1/2}$ |
| Recombination rates: |
| $\alpha_{H^+} = 8.4 \times 10^{-11}(1 + T_{e6}^{0.7})^{-1} T_e^{-1/2} T_{e3}^{-0.2}$ |
| $\alpha_{He^+} = 1.5 \times 10^{-10} T_e^{0.6353}$ |
| $\alpha_{He^{++}} = 3.36 \times 10^{-10}(1 + T_{e6}^{0.7})^{-1} T_e^{-1/2} T_{e3}^{-0.2}$ |

where $\beta_i$ and $\alpha_i$ are the ionization and recombination rates presented in Table 1, and the conservation equations:

$$n_{H^0} + n_{H^+} = n_H, \tag{8}$$

$$n_{He^0} + n_{He^+} + n_{He^{++}} = n_{He}, \tag{9}$$

$$n_{H^+} + n_{He^+} + 2n_{He^{++}} = n_e. \tag{10}$$

The number densities of the six species allow computation of cooling rates and since the numerical code allows ions, neutrals and electrons to have their own temperature, cooling rates depend on electron temperature and are detailed in Table 2.

Energy transfers between the three populations are expressed by:

$$Q_{x_1,\,x_2} = -Q_{x_2,\,x_1} = \frac{(n_{x_1}/n_{x_2})e_{x_2} - e_{x_1}}{\tau_{x_1,\,x_2}}, \tag{11}$$

where $\tau_{x_1,\,x_2}$ is the characteristic timescale of interaction between $x_1$ and $x_2$ species. The energy exchange between electrons and ions is due to Coulomb interactions and the exchange timescale is (Spitzer 1962):

$$\tau_{e,\,ion}(s) \approx 251.5\,\frac{A\,T_e^{3/2}}{n_e\,\ln(\Lambda)}, \tag{12}$$

where $A$ the molecular weight, $T_e$ the electronic temperature and $\ln(\Lambda)$ the Coulomb logarithm. The energy exchange between electrons and neutrals is due to short-range forces and, using the classical "hard reflecting sphere" cross-section $\sigma_{e,\,neut} \approx 10^{-15}$ $cm^2$ (Draine & Katz 1986), the exchange timescale can be written as (Zel'dovich & Raizer 1966):

$$\tau_{e,\,neut}(s) \approx \frac{A}{4.5 \times 10^{-13}\,n_n\,T_e^{1/2}}. \tag{13}$$

The energy exchange timescale between ions and neutrals is very short compared to the other timescales above. It is worth noting that the term $Q_{exch}$ represents an energy gain for electrons and an energy loss for the heavy particles.

The simulations are performed for a flat $\Lambda$-dominated cold dark matter model defined by $\Omega_m = 0.3$, $\Omega_\Lambda = 0.7$, $\Omega_b h^2 = 0.02$, $h = (H_0/100) = 0.7$. The transfer function is taken from Bardeen et al. (1986) with a shape parameter from Sugiyama (1995). We use the normalization on COBE data (Bunn & White 1997) giving at $R = 8\ h^{-1}$ Mpc a filtered dispersion $\sigma_8 = 0.91$. The computational cubic volume

**Table 2.** Cooling rates expressed in erg $s^{-1}$ $cm^{-3}$ (from Black (1981) with modifications introduced by Cen (1992) for temperatures exceeding $10^5$ K) with $T_{en} = T_e/10^n$ K the electron temperature, $g_{ff}$ the Gaunt factor taken to 1.5, and $T_{bg}$ the cosmic microwave background temperature, $T_{bg} = 2.7(1 + z)$.

| Collisional excitation: |
|---|
| $\Lambda_{H^0} = 7.5 \times 10^{-19}(1 + T_{e5}^{1/2})^{-1} e^{(-118348/T_e)} n_e n_{H^0}$ |
| $\Lambda_{He^+} = 5.54 \times 10^{-17}(1 + T_{e5}^{1/2})^{-1} e^{(-473638/T_e)} T_e^{-0.397} n_e n_{He^+}$ |
| Collisional ionization: |
| $\Lambda_{H^0} = 1.27 \times 10^{-21}(1 + T_{e5}^{1/2})^{-1} e^{(-157809.1/T_e)} T_e^{1/2} n_e n_{H^0}$ |
| $\Lambda_{He^0} = 9.38 \times 10^{-22}(1 + T_{e5}^{1/2})^{-1} e^{(-285335.4/T_e)} T_e^{1/2} n_e n_{He^0}$ |
| $\Lambda_{He^+} = 4.95 \times 10^{-22}(1 + T_{e5}^{1/2})^{-1} e^{(-631515/T_e)} T_e^{-0.397} n_e n_{He^+}$ |
| Recombination: |
| $\Lambda_{H^+} = (3/2)kT_e \times 8.4 \times 10^{-11}(1 + T_{e6}^{0.7})^{-1} T_e^{1/2} T_{e3}^{-0.2} n_e n_{H^+}$ |
| $\Lambda_{He^+} = (3/2)kT_e \times 1.5 \times 10^{-10} T_e^{0.3647} n_e n_{He^+}$ |
| $\Lambda_{He^{++}} = (3/2)kT_e \times 3.36 \times 10^{-10}(1 + T_{e6}^{0.7})^{-1} T_e^{1/2} T_{e3}^{-0.2} n_e n_{He^{++}}$ |
| Bremsstrahlung: |
| $\Lambda_{ff} = 1.42 \times 10^{-27} g_{ff} T_e^{1/2}(n_{H^+} + n_{He^+} + 4n_{He^{++}}) n_e$ |
| Compton interaction: |
| $\Lambda_C = 5.65 \times 10^{-36}(1 + z)^4 (T_e - T_{bg}) n_e$ |

is of 16 comoving $h^{-1}$ Mpc on a side with $N_g = 256^3$ grid cells and $N_p = 256^3$ dark matter particles allowing a spatial resolution of 62.5 $h^{-1}$ kpc. The dark matter particle mass is $M_{dm} = 2.51 \times 10^7\ M_\odot$ and the gas mass resolution is $M_{bm} = 3.87 \times 10^6\ M_\odot$. In Sect. 3.1, the simulations are 32 comoving $h^{-1}$ Mpc on a side with other parameters similar.

We refer to simulations with non-equipartition processes as $S_{3T}$ and the results are compared with simulations in which equipartition processes are forced. In that case the three species have the same temperature and these simulations are denoted $S_{1T}$.

## 3. Thermodynamic properties of baryons

Accretion of baryons into potential wells created by dark matter involves gravitational compression and hydrodynamical shocks. Dissipative processes convert the kinetic energy of the cosmological plasma into thermal energy and the increase in temperature depends on the particle mass (Eq. (19)). Owing to the large difference of mass between electrons and heavy particles (ions and neutral atoms), the energy transfer between these species is poorly efficient, leading to an out of equilibrium plasma. The next two subsections describe the thermodynamic evolution of the cosmological plasma, first inside high mass structures comparable to galaxy clusters and, secondly inside low mass structures comparable to proto-galaxies.

### 3.1. High mass structures or totally ionized IGM

Figure 1 focuses on a high mass structure in the $S_{3T}$ simulation and displays electron and ion temperature distributions. This cluster-like structure is extracted from a large scale field at $z = 0$. Isocontours illustrates shock heated baryonic matter at temperatures around $10^7$–$10^8$ K which is typically the

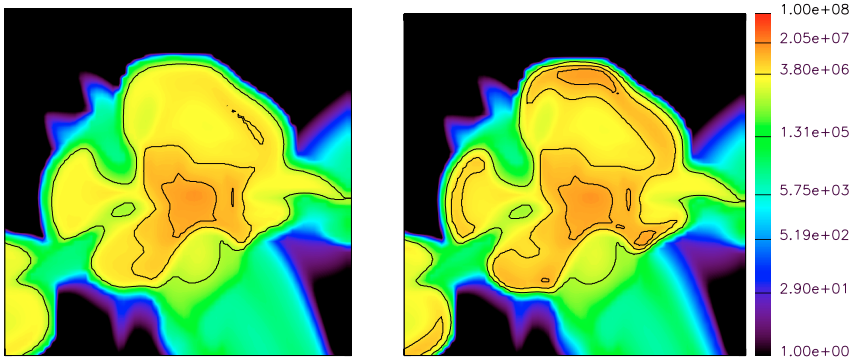


**Fig. 1.** Isocontours of electron (*left panel*) and heavy particle (*right panel*) temperatures for a high mass structure extracted from the large scale $S_{3T}$ simulation including non-equipartition processes (the slices are 8 comoving $h^{-1}$ Mpc on a side and contour levels are: $10^6, 5\times10^6, 10^7, 2\times10^7, 5\times10^7, 10^8$ K).

hot intra-cluster medium temperature. Indeed, galaxy clusters result from the merger of sub-units of matter inside deep potential wells created by the large scale collapse of dark matter. Hydrodynamic shocks induced by mergers heat the heavy particles to high temperatures and in the outer regions, just behind the shock fronts, the electron temperature is significantly lower than the ion temperature.

In the case of discontinuities, the post-shock temperature for each species of the plasma is computed with the conservation equations which connect impulsion, $\rho u$, pressure, $p$, and specific enthalpy, $h = H/\rho$, on both sides of the thin compression region. Ions and neutral particles are grouped under the term heavy particles with the subscript HP. Pre-shock quantities in the unperturbed region are denoted with the subscript 0 and no subscript is reserved for post-shock quantities. The Rankine-Hugoniot relations, written with the compression ratio $\omega = \rho_0/\rho$, are:

$$\rho u = \rho_0 u_0, \tag{14}$$

$$p = \rho_0 u_0^2(1-\omega) + p_0, \tag{15}$$

$$h = \frac{1}{2}u_0^2(1-\omega^2) + h_0. \tag{16}$$

The specific enthalpy for the plasma is expressed by:

$$h = \frac{1}{\rho}\left(\frac{5}{2}n_{\rm HP}kT_{\rm HP} + \frac{5}{2}n_{\rm e}kT_{\rm e}\right), \tag{17}$$

with $n_{\rm e}$ and $n_{\rm HP}$ the number densities of the electrons and the heavy particles, respectively, and $T_{\rm e}$ and $T_{\rm HP}$ the electron and the heavy particle temperatures, respectively. The increase in temperature is then calculated by assuming that the number density per mass unit for each species ($n_x/\rho$) is constant across the discontinuity:

$$T_{\rm HP} - T_{\rm HP_0} = \frac{n_{\rm e_0}}{n_{\rm HP_0}}(T_{\rm e_0} - T_{\rm e}) + \frac{\rho_0 u_0^2\left(1-\omega^2\right)}{5kn_{\rm HP_0}}. \tag{18}$$

The electron gas undergoes adiabatic compression across the discontinuity and the electron temperature increases by a factor of $1/\omega^{\gamma-1}$ (Zel'dovich & Raizer 1966). The variation $(T_{\rm e_0} - T_{\rm e})$ can then be neglected in Eq. (18). Moreover for strong shocks, $1/\omega \approx 4$, and the last term becomes $\approx(3/16)(\rho_0\mathcal{D}^2/(kn_{\rm HP_0}))$. By introducing the molecular weight of the gas $A$, the increase in temperature for heavy particles becomes:

$$\Delta T_{\rm HP} \approx \frac{3}{16}\frac{Am_{\rm p}}{k}u_0^2, \tag{19}$$

$$\approx 2.2\times10^5\ {\rm K}\left(A\cdot\frac{\mathcal{D}}{100\ {\rm km\ s^{-1}}}\right)^2. \tag{20}$$

As gravitational compression and shocks heat preferentially the heavy particles, the temperature of the two species can differ significantly in an extended relaxation layer during a timescale which depends on the energy transfer between particles. Plasma in galaxy clusters is fully ionized and for typical values of density and temperature in outer regions, an estimate of the characteristic timescale for the energy exchange between electrons and ions gives (see Eq. (12)):

$$\tau_{\rm e,\ ion} \approx 9.4\times10^9\ {\rm yr}\ \frac{(T_{\rm e}/5\times10^7\ {\rm K})^{3/2}}{(n_{\rm e}/10^{-5}\ {\rm cm^{-3}})\,(\ln(\Lambda)/30)}. \tag{21}$$

This relaxation timescale is of the order of the Hubble time $\tau_{\rm H}$, and explains the departure from equilibrium in the outer regions such as seen in Fig. 1. For higher density, this timescale decreases and the equilibrium can be rapidly recovered between both species: the distributions in Fig. 1 show that, in the structure center, both temperatures are similar. A number of earlier studies show such differences between temperatures in galaxy cluster high-resolution simulations based on Hoffman-Ribak initial conditions (Chièze et al. 1998; Takizawa & Mineshige 1998; Takizawa 1998). Here we reach similar conclusions but obtained using simulations of large scale structure formation.

Departure from equilibrium in the outer regions of a massive galaxy cluster is a first illustration of the influence of non-equipartition processes on the IGM. However, in hierarchical models massive galaxy clusters exist mainly at low redshifts and an out of equilibrium plasma at temperature higher than $10^7$ K is only expected at these redshifts. We now analyze the influence of non-equipartition processes on the cosmological plasma over the evolution of the universe, at epochs when a larger fraction of baryonic matter is contained in low mass structures.

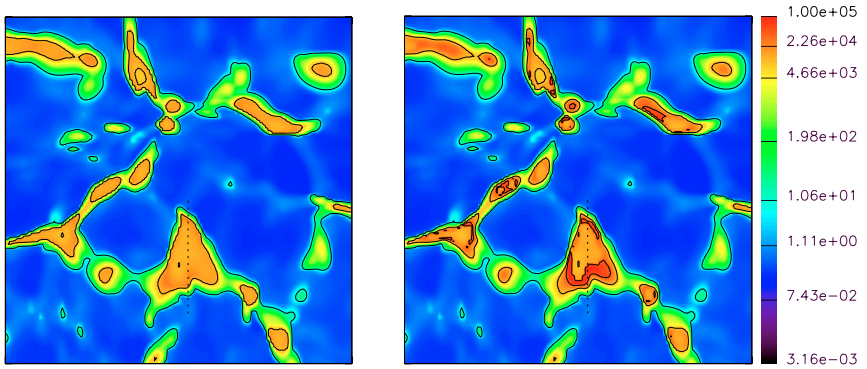


**Fig. 2.** Isocontours of the gas temperature in the $S_{1T}$ simulation (*left panel*) and the heavy particle temperature in the $S_{3T}$ simulation (*right panel*) at $z = 4$ (the slices are 8 comoving $h^{-1}$ Mpc on a side and contour levels are: 10, $10^4$, $4 \times 10^4$ K).

### 3.2. Low mass structures or weakly ionized IGM

Figure 2 illustrates departure from equilibrium in structures much less massive than galaxy clusters and at high redshift. Temperature distributions for a typical region show significant differences between the simulation with non-equipartition processes and the simulation in which equipartition is forced between species: heavy particle temperature in the $S_{3T}$ simulation is larger than plasma temperature in the $S_{1T}$ simulation. These differences are located in the outer regions of bound structures and are in the range $10^4$–$10^6$ K.

Figure 3 displays the temperature profiles along a line of sight through one of the structures shown on the temperature distributions in Fig. 2 (the line of sight is marked by the dashed line). The outer parts of the profiles show that, in the $S_{3T}$ simulation, the heavy particle temperature rises up to $10^5$ K whereas the electron temperature is around $10^4$ K. In the same regions but for the $S_{1T}$ simulation the plasma temperature is at a few times $10^4$ K. Then in the range of temperature $10^4$–$10^5$ K, the IGM in the $S_{3T}$ simulation is significantly warmer than in the $S_{1T}$ simulation.

Figure 3 plots also the ionization degree profiles along the same line of sight. The ionization degree is defined by $x = n_e/(n_H + n_{He})$. These profiles point out that in the regions of temperature differences (clearly seen on the left side of the profiles), the plasma is weakly ionized in the $S_{3T}$ simulation whereas it is partially ionized in the $S_{1T}$ simulation. The former being two orders of magnitude lower than the latter.

We now quantitatively estimate the mass fraction of that warmer plasma. First of all the baryonic mass fraction per interval of heavy particle temperature and per interval of electron temperature is computed in the $S_{3T}$ simulation at different redshifts. Figure 4 shows that the baryonic mass fraction with heavy particle temperature between $10^4$–$2 \times 10^5$ K is larger than the baryonic mass fraction with electron temperature in the same range. That warm out of equilibrium plasma exists at any redshift but its mass fraction decreases with redshift.

To inquire about the density of the warm plasma, we plot in Fig. 5 isocontours of the baryonic mass fraction per interval of temperature and per interval of baryonic density contrast $\delta_b = \rho_b/\langle\rho_b\rangle$. The diagram on the left, as a function of the heavy particle temperature, shows a region with temperatures in the range $2 \times 10^4$–$5 \times 10^5$ K and baryonic density contrasts

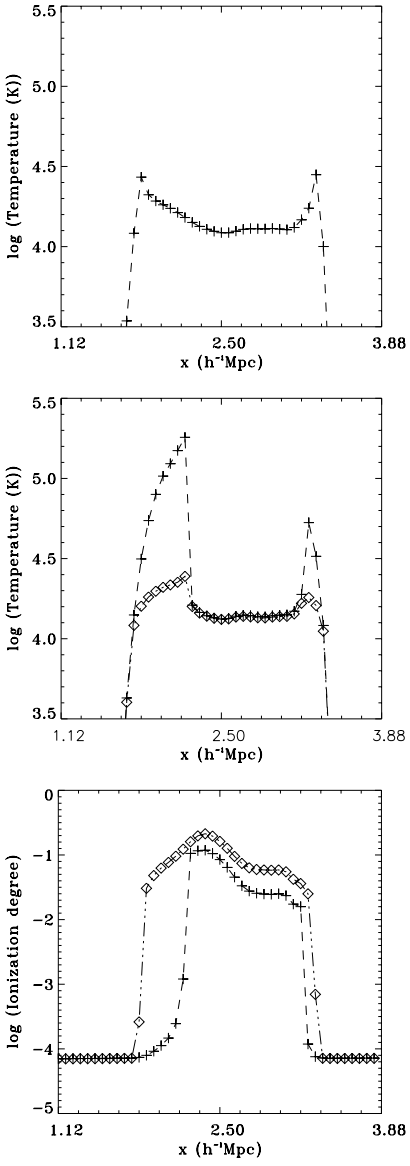


**Fig. 3.** Temperature and ionization degree profiles along the line of sight marked by the dashed line in Fig. 2: gas temperature in the $S_{1T}$ simulation (*top panel*), heavy particle temperature (*middle panel*, plus sign), electron temperature (*middle panel*, diamond sign), ionization degree in the $S_{3T}$ simulation (*bottom panel*, plus sign), ionization degree in the $S_{1T}$ simulation (*bottom panel*, diamond sign).

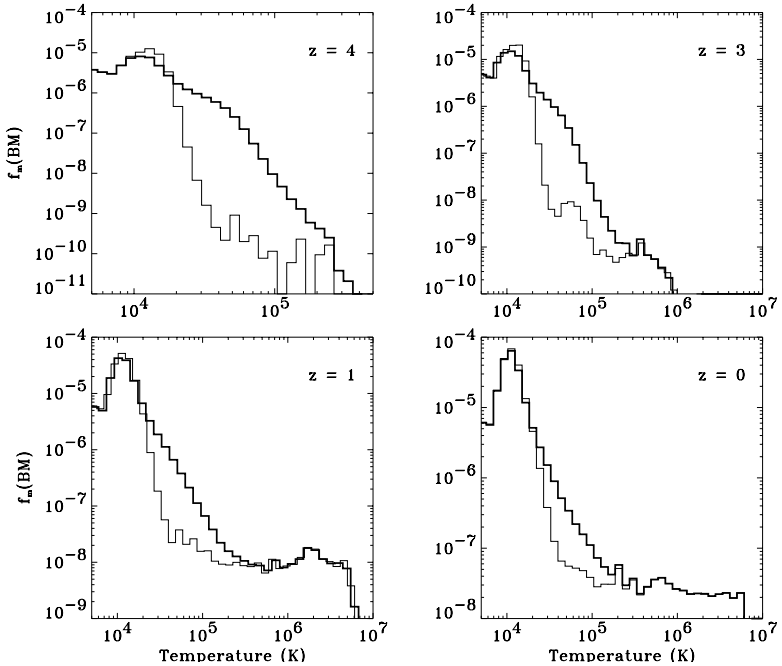


**Fig. 4.** Baryonic mass fraction per interval of electron temperature (thin line) and per interval of heavy particle temperature (thick line) at different redshifts in the $S_{3T}$ simulation.

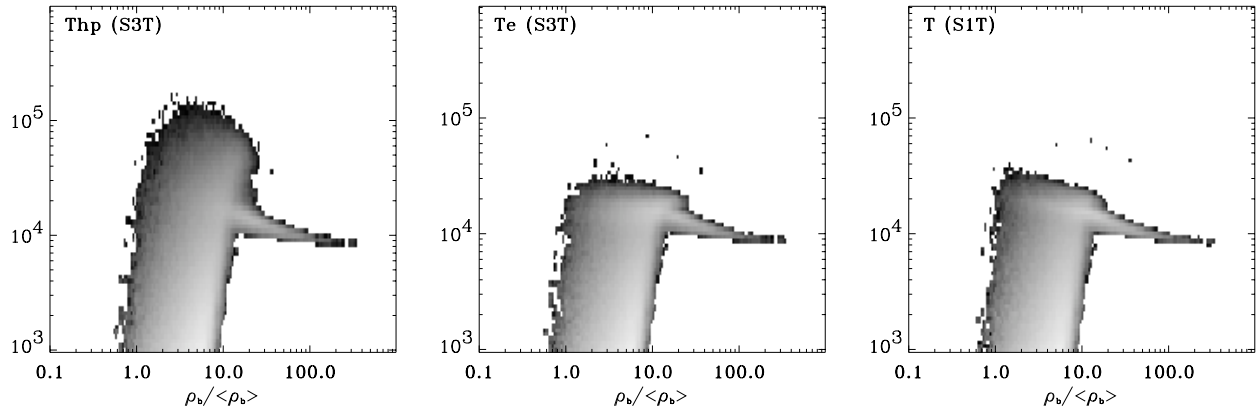


**Fig. 5.** Baryonic mass fraction at $z = 5$ per interval of baryonic density contrast and per interval of heavy particle temperature (*left panel*), per interval of electron temperature (*middle panel*) in the $S_{3T}$ simulation, per interval of gas temperature in the $S_{1T}$ simulation (*right panel*), light grey is high mass fractions and temperature is shown on the ordinate axis.

around 10 or less. The middle plot shows that electron temperature in this region is a few times $10^4$ K. The point here is that this warm plasma region is not found in the $S_{1T}$ simulation where the plasma is rather cold (right panel). Differences between the two simulations are then identified by a warm temperature plasma with relatively low baryonic density contrast.

Finally we estimate the evolution with redshift of the different phases of the plasma in the $S_{3T}$ simulation and compare with the $S_{1T}$ simulation. We define a bulk plasma temperature in the former simulation as:

$$T_g = \frac{(s_e + s_i + s_n)V_s^{-2/3}}{\frac{3}{2}kN_{tot}} \equiv \frac{n_e T_e + n_i T_i + n_n T_n}{n_e + n_i + n_n} \quad (22)$$

where $N_{tot}$ is the total number of particles. The evolution of the baryonic mass fraction is computed for different ranges of temperature, $T_g$ in $S_{3T}$ and $T$ in $S_{1T}$. Mass fractions are normalized to the total baryonic mass with a temperature higher than $9 \times 10^3$ K. Three ranges of temperatures are considered: $9\times10^3 \leq T < 2\times10^4$ K, $2\times10^4 \leq T < 5\times10^5$ K and $T \geq 5\times10^5$ K. Figure 6 shows that, between $z = 7$ and $z = 3$, about 30–40% of the plasma is warm ($2\times10^4 \leq T < 5\times10^5$ K) in the $S_{3T}$ simulation whereas this phase represents only less than 5% in the $S_{1T}$ simulation. We note that, in particular at high redshift, the plasma that is warm in the $S_{3T}$ simulation is cold ($9 \times 10^3 \leq T < 2 \times 10^4$ K) in the $S_{1T}$ simulation, and that the cold baryonic mass fraction is much lower in the $S_{3T}$ simulation (this point will be addressed in the final section).

### 3.3. Influence of the viscous dissipation function

Before deducing any cosmological implications from the thermodynamic and chemical differences between the two simulations as described in the previous section, we have to check that

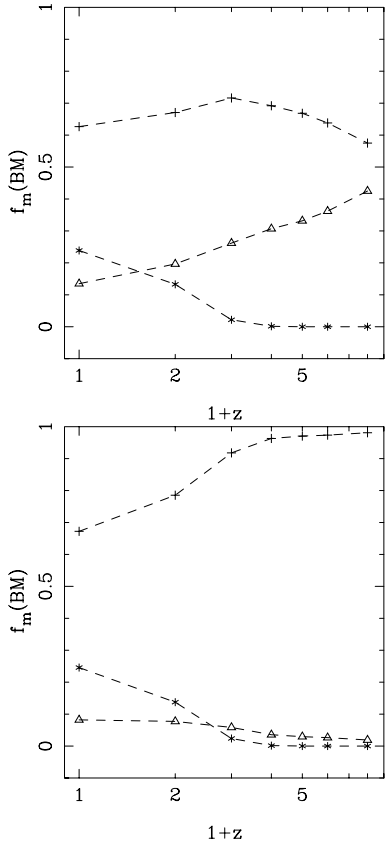


**Fig. 6.** Evolution with redshift of the baryonic mass fraction computed for different ranges of temperature (normalized to the total baryonic mass with a temperature higher than $9 \times 10^3$ K): $9 \times 10^3 \leq T < 2 \times 10^4$ K (plus sign), $2 \times 10^4 \leq T < 5 \times 10^5$ K (triangle), $T \geq 5 \times 10^5$ K (star), in the $S_{3T}$ (upper panel) and $S_{1T}$ (lower panel) simulations.

our results are not due to numerical effects. In fact the pseudo-entropy equation (Eq. (2)) computes the contribution to the energy of shocks and gravitational compression and includes a numerical heating term given by the artificial viscosity. Is this term responsible for departure from equilibrium seen in the $S_{3T}$ simulation? To invalidate this hypothesis, we run the same simulations except that now the constants $C_1$ and $C_2$ in the term $Q_v$ (Eq. (3)) are reduced by a factor 10.

Figure 7 plots the same temperature field as in Fig. 2 for heavy particles in the $S_{3T}$ simulation and for plasma temperature in the $S_{1T}$ simulation. The temperature profiles are also displayed along the same line of sight as before. Temperature distribution in the $S_{1T}$ simulation shows that, due to the reduction of the shock contribution, the amount of energy created by shocks is lower resulting in a too low pressure to support gravitational compression. The spatial extension of structures are then globally smaller than in Fig. 2.

Nonetheless, comparing the two simulations reveals that the $S_{3T}$ simulation shows also a substantial fraction of the IGM warmer than in the $S_{1T}$ simulation and regions which depart from equilibrium in the outer regions of bound structures are spatially larger than the region over which the artificial viscosity is applied. We can conclude that the heating of heavy particles is not dominated by numerical effects. Moreover as will be pointed out in Sect. 5.1, increasing the resolution but keeping the same value for the viscous term used in Sect. 3.2, leads also to departure from equilibrium. The thermodynamic differences between the $S_{3T}$ and $S_{1T}$ simulations are then of physical origin and examined in the next section.

## 4. Analytical interpretation

In the outer regions of not too dense structures, the IGM is out of equilibrium for temperatures in the range $10^4$–$10^6$ K and is weakly ionized (Figs. 2 and 3). Contrary to the outer regions of galaxy clusters in which the IGM is totally ionized and with sufficiently high density to give a relaxation timescale of the order of the Hubble time (see Eq. (21)), relaxation timescales between ions and electrons and between neutrals and electrons are now very short compared to the Hubble time:

$$\tau_{\mathrm{e,\ ion}} \ll \tau_{\mathrm{e,\ neut}} \ll \tau_{\mathrm{H}}. \tag{23}$$

We take into account interactions between neutrals and electrons since the plasma is weakly ionized.

What are the mechanisms which control departure from equilibrium and is the relaxation timescale long enough to allow physical effects on cosmological time? This section provides answers to these questions based on a semi-analytical model.

We consider here the relaxation of an out of equilibrium hydrogen plasma having just undergone gravitational compression. Relaxation processes are cooling and non-equipartition processes. We neglect other processes such as the expansion of the universe or compression due to the accretion of matter or merger events. The plasma is composed of hydrogen nuclei (neutrals and ionized particles) and electrons with number densities $n_{\mathrm{H}} \equiv n_{\mathrm{HP}} = n_{\mathrm{H^0}} + n_{\mathrm{H^+}}$ and $n_{\mathrm{e}}$, respectively. Densities can be expressed with the ionization degree $x$:

$$n_{\mathrm{e}} = x n_{\mathrm{H}} \equiv n_{\mathrm{H^+}} \text{ and } n_{\mathrm{H^0}} = n_{\mathrm{H}}(1 - x). \tag{24}$$

Initial conditions are suggested by the results of the simulations: temperatures of heavy particles and electrons are respectively, $T_{\mathrm{HP}} = 10^5$ K and $T_{\mathrm{e}} = 2{\times}10^4$ K, hydrogen nuclei density is $n_{\mathrm{H}} = 5 \times 10^{-5}$ cm$^{-3}$ and the ionization degree is $x = 10^{-4}$.

We solve an equation of energy balance for heavy particles and for electrons:

$$\left(\frac{\mathrm{d}e}{\mathrm{d}t}\right)_{\mathrm{HP}} = -\frac{1}{\rho} Q_{\mathrm{exch}}, \tag{25}$$

$$\left(\frac{\mathrm{d}e}{\mathrm{d}t}\right)_{\mathrm{e}} = +\frac{1}{\rho} Q_{\mathrm{exch}} - \frac{1}{\rho} Q_{\mathrm{cool}}, \tag{26}$$

where the right hand terms represent the change in the specific internal energy for the two fluids. $Q_{\mathrm{cool}}$ is the rate of energy lost by the electrons (per unit of volume and per unit of time):

$$Q_{\mathrm{cool}} = \Lambda_{\mathrm{exc}}(\mathrm{H}) + \Lambda_{\mathrm{ion}}(\mathrm{H}) + \Lambda_{\mathrm{rec}}(\mathrm{H}) + \Lambda_{\mathrm{brem}}(\mathrm{H}). \tag{27}$$

The cooling rates associated with each process, collisional excitation, collisional ionization, recombination, bremsstrahlung,

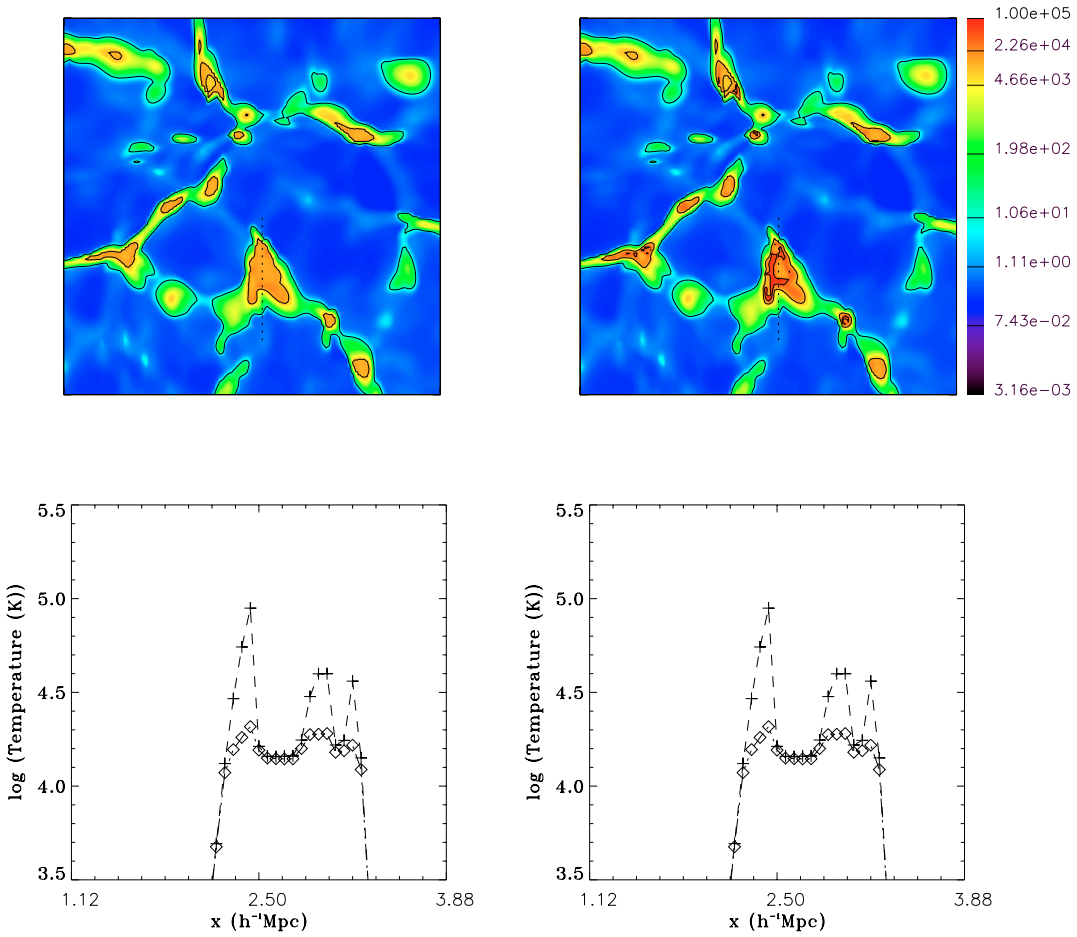


**Fig. 7.** Influence of the viscous dissipation function: the $S_{3T}$ and the $S_{1rmT}$ simulations are now computed with the $Q_v$ term (Eq. (3)) reduced by 10. *Upper panels*: isocontours of gas temperature in the $S_{1T}$ simulation (*left panel*) and of heavy particle temperature in the $S_{3T}$ simulation (*right panel*) for the same field as in Fig. 2 (isocontours at 10, $10^4$, $4\times10^4$ K). Bottom panels: temperature profiles along the line of sight shown on top panels by the dashed line: gas temperature in the $S_{1T}$ simulation (*left panel*), heavy particle temperature (*right panel*, plus sign), electron temperature (*right panel*, diamond sign).

are given in Table 2. $Q_{exch}$ is the rate of energy exchange between electrons and heavy particles (per unit of volume and per unit of time):

$$Q_{exch} = \frac{3}{2} k n_e \frac{(T_{HP} - T_e)}{\tau_{exch}}, \tag{28}$$

where $\tau_{exch}$ includes two terms due to two interaction mechanisms, that between charged particles and between neutral and charged particles:

$$\frac{1}{\tau_{exch}} = \frac{1}{\tau_{e,\,ion}} + \frac{1}{\tau_{e,\,neut}}. \tag{29}$$

We consider isochoric transformations, $d\rho/dt = 0$, then, since $\rho \approx m_p n_H$ with $m_p$ the atomic mass, $dn_H/dt = 0$ and Eqs. (25) and (26) become:

$$\frac{3}{2} k n_H \frac{dT_{HP}}{dt} = -Q_{exch}, \tag{30}$$

$$\frac{3}{2} k n_e \frac{dT_e}{dt} = +Q_{exch} - Q_{cool} - \frac{3}{2} k T_e n_H \frac{dx}{dt}, \tag{31}$$

where $x$ is the ionization degree. The last term of the second equation is computed from the evolution equation of the electron density:

$$\frac{dn_e}{dt} = n_H \frac{dx}{dt} = \beta_{H^0} n_e n_{H^0} - \alpha_{H^+} n_e n_{H^+}, \tag{32}$$

where $\beta_{H^0}$ and $\alpha_{H^+}$ are respectively the ionization and recombination rates for hydrogen (see Table 1). We compute the evolution of $T_e$, $T_{HP}$ and $x$ with respect to time using Eqs. (30)–(32).

Figure 8a shows that departure from equilibrium is maintained on a timescale of gigayears, and that during this time the ionization degree does not evolve (Fig. 8b). It is interesting to note that just before the equilibration between the two temperatures, the electron temperature slightly increases because of the energy gained in elastic processes[2]. Figure 8c presents the evolution of the different characteristic times: the energy exchange timescale between electrons and ions (Eq. (12)), the energy exchange timescale between electrons and neutrals (Eq. (13)),

[2] Similar evolutions were computed in a sophisticated analysis by Fadeyev & Gillet (1998), of the structure of radiative shock waves propagating in stellar envelopes.

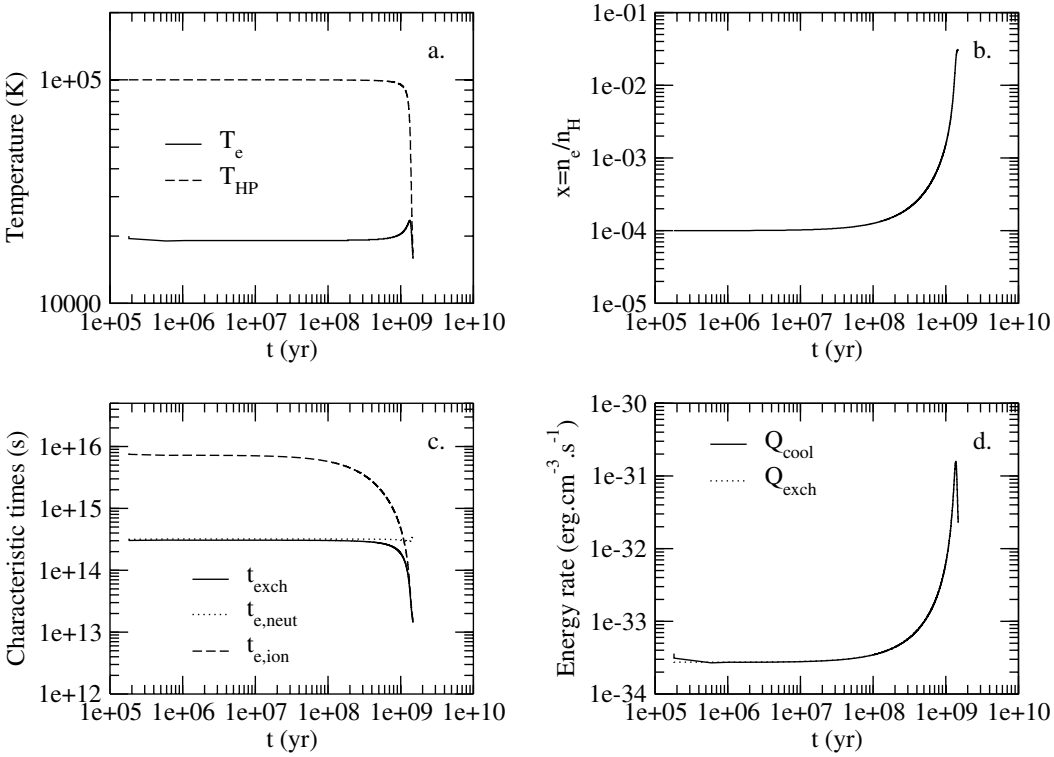


**Fig. 8.** Temporal evolution of heavy particle and electron temperatures **a)**, ionization degree **b)**, characteristic times **c)**, and energy exchange and cooling rates **d)** using Eqs. (30)–(32).

and the resultant $\tau_{\rm exch}$ due to both mechanisms (Eq. (29)). It is interesting to see that in the relaxation region and since the plasma is weakly ionized, elastic processes are dominated by neutral-electron interactions and $\tau_{\rm exch} \approx \tau_{\rm e,\ neut}$. Equilibration is recovered once plasma is getting partially ionized and during this short period, $\tau_{\rm exch} \approx \tau_{\rm e,\ ion}$. Once the ionization degree increases, $\tau_{\rm exch}$ decreases drastically and equipartition is established.

Moreover, Fig. 8d shows that the energy exchange rate between heavy particles and electrons is approximately equal to the cooling rate. This means that there is no change in the electronic internal energy (Eq. (26)). By writing $Q_{\rm exch} \approx Q_{\rm cool}$ we then derive a relation between $T_{\rm HP}$ and $T_{\rm e}$ such as:

$$T_{\rm HP} = T_{\rm e} + \left(\frac{3}{2}\frac{kn_{\rm e}}{\tau_{\rm exch}^{-1}}\right) Q_{\rm cool}. \qquad (33)$$

Since $Q_{\rm cool} = f(T_{\rm e}, n_{\rm e}, n_{\rm H^0}, n_{\rm H^+})$ this relation is only parameterized by the ionization degree[3]. In Fig. 9a we plot $T_{\rm HP}$ as evaluated in Eq. (33), with the cooling term given by Eq. (27), for different values of the ionization degree. In a narrow electronic temperature range, $10^4$–$3 \times 10^4$ K, the heavy particle temperature extends in a much larger range, between $10^4$ and $5 \times 10^5$ K. It is interesting to note that the higher the value of the ionization degree, the smaller is the difference between the two temperatures. For very low ionization degree the relation between $T_{\rm HP}$ and $T_{\rm e}$ does not depend on $x$ since $\tau_{\rm e,\ neut} \propto (n_{\rm H^0} T_{\rm e}^{1/2})^{-1}$, and Fig. 8c shows that departure from equilibrium in weakly ionized plasma is controlled by neutral-electron mechanisms.

[3] This approach was used by Petschek & Byron (1957) to determine the ionization rate of a gas of argon in a shock tube.

In this range of electronic temperatures, cooling via bremsstrahlung processes is not efficient, and neither is cooling due to recombination processes (too low density). Then only terms due to collisional excitation and collisional ionization processes are effective in Eq. (27). Figure 9b illustrates the relation between $T_{\rm HP}$ and $T_{\rm e}$ when Eq. (33) is solved by neglecting the collisional excitation term. We note that even in that case, departure from equilibrium is also seen, but now for higher electron temperatures.

Then for a given ionization degree and electron temperature slightly higher than $10^4$ K, the energy exchange rate between the heavy particles and the electrons compensates for the energy lost by the electron gas due to inelastic processes. We now return to the $S_{3\rm T}$ simulation and confirm this scenario by plotting temperature values for heavy particles and electrons in each cell of the computational volume. Each symbol in Fig. 10 corresponds to the range of ionization degree of each cell of the simulation. We overplot relation (33) for different ionization degrees. For instance squares indicate cells with ionization degree between $10^{-3} < x \leq 10^{-2}$, and we see that these cells are in the region delimited by the curves $x = 10^{-3}$ and $x = 10^{-2}$. The agreement for each range of ionization validates the condition $Q_{\rm exch} \approx Q_{\rm cool}$. These results confirm our understanding of the physical origin of the non-equilibrium IGM in moderately dense structures, although numerical simulations include a larger set of physical processes (as expansion and accretion).

Departure from equilibrium results from the competition between elastic processes in the weakly ionized IGM and cooling processes. It is clear that the thermodynamic history of

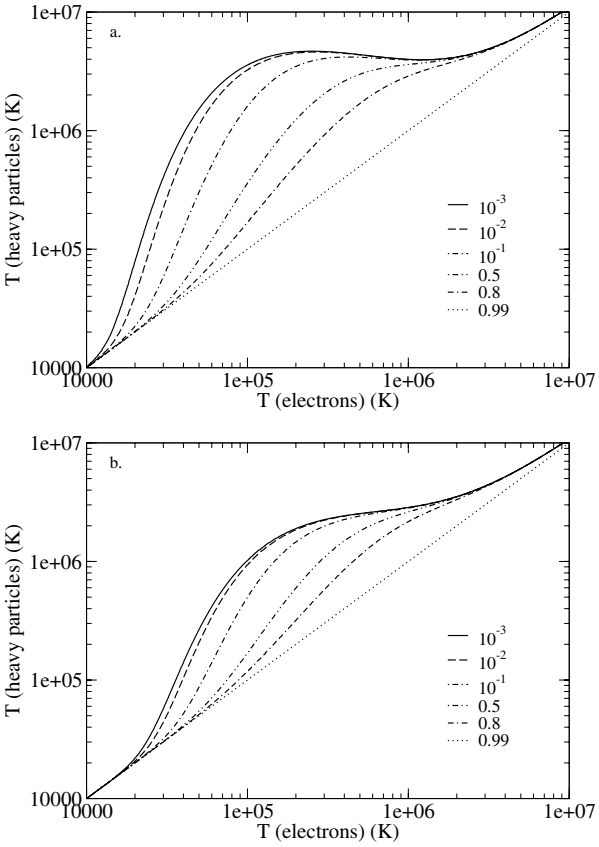


**Fig. 9.** Heavy particle temperature versus electron temperature for different values of the ionization degree computed by Eq. (33) with **a)** and without **b)** collisional excitation cooling term in Eq. (27).

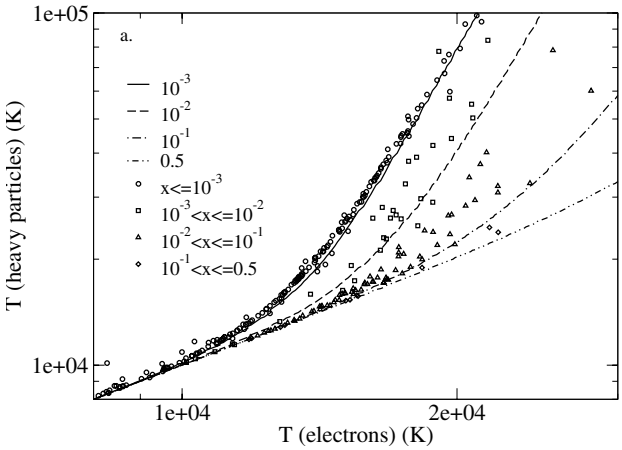


**Fig. 10.** Heavy particle temperature versus electron temperature at $z = 3$ in 300 cells randomly chosen in the $S_{3T}$ simulation; each symbol represents the ionization degree in each cell and the curves are computed in the same way as in Fig. 9a.

accreted gas in bound structures is not the same in a simulation with non-equipartition processes and in a simulation in which equipartition is forced. As the plasma undergoes gravitational compression in not too dense structures, heavy particles are heated much more than the electrons. The electron temperature does not increase sufficiently to partially ionize the medium (see also the evolution of temperature and ionization degree in Fig. 8). Therefore the ionization degree profiles in the outer regions in the $S_{3T}$ simulation (Fig. 3) show a weakly ionized plasma with $T_e \sim 10^4$ K. But in the $S_{1T}$ simulation the electrons can be heated up to $2 \times 10^4$ K, and though the ionization temperature of hydrogen is, with $I$ the ionization potential, $T = I/k \sim 1.6 \times 10^5$ K, a plasma at $T \simeq 2 \times 10^4$ K is ~90% ionized (Shchekinov 1991). The ionization degree of a hydrogen plasma in collisional ionization equilibrium is $\beta_{H^0}/(\beta_{H^0} + \alpha_{H^+})$. This fact explains the two orders of magnitude difference between the ionization degree profiles plotted for the $S_{3T}$ and the $S_{1T}$ simulations (at $1.5 \times 10^4$ K, the ionization rate for hydrogen is $\sim 10^{-13}$ s$^{-1}$ cm$^3$ whereas at $2.5 \times 10^4$ K the ionization rate is $\sim 10^{-11}$ s$^{-1}$ cm$^3$).

Before closing this section, we would like to mention an interesting point. In the center of structures such as in Fig. 2, the IGM is cold and partially ionized in the $S_{1T}$ simulation (Fig. 3). This suggests that in such not too dense structures the IGM can be never heated to the so-called virialized temperature and can be partially ionized and radiate its energy just by being heated up to $3 \times 10^4$ K. This is supporting evidence to the important question recently summarized by Katz et al. (2002) concerning results from different numerical simulations of large scale structure formation, showing that a non-negligible fraction of the accreted gas can never reach the virialized temperature (Katz & Gunn 1991; Kay et al. 2000; Fardal et al. 2001).

## 5. Cosmological implications

The introduction of non-equipartition processes alters, for not too dense structures, the properties of plasma with temperature in the range $10^4$–$10^6$ K. This plasma is expected to contribute to galaxy formation. In this section we qualitatively analyze the influence of non-equipartition processes on galaxy formation. We discuss when and how this influence is dominant.

### 5.1. At high redshift

The analytical interpretation shows that the weaker the plasma is ionized the larger the departure from equilibrium. Figure 9 shows that the difference between heavy particle and electron temperature (in the range $10^4$–$10^6$) is larger for lower ionization degree and Fig. 8 shows that decoupling is mainly due to interaction mechanisms between neutrals and electrons. This suggests that two conditions are required for a not too dense plasma to be out of equilibrium. The first one is that the plasma accreted into structures must be weakly ionized. The second one is that cooling processes must involve atomic cooling (collisional excitation and/or collisional ionization). This suggests that the major influence of the non-equipartition processes occurs before the end of the reionization epoch, i.e. at epochs when the cosmological plasma is not fully ionized and when the cooling is dominated by atomic cooling.

To numerically confirm this point, we introduce photoionization processes in the $S_{3T}$ and the $S_{1T}$ simulations to see what happens after complete reionization of the universe. As the analysis of the influence of photoionization processes is

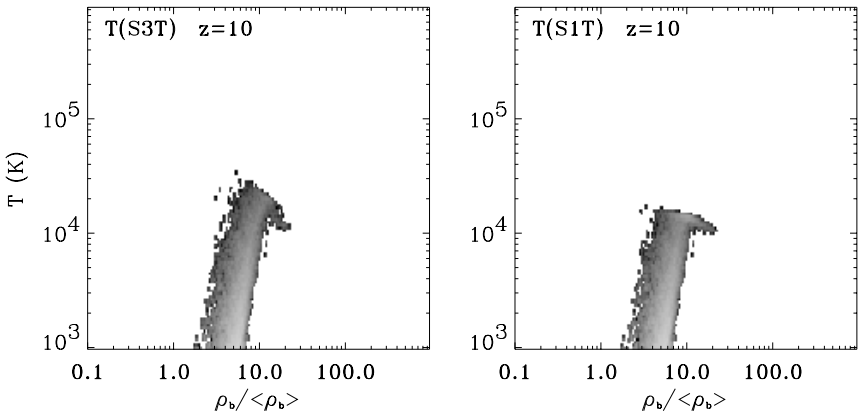


**Fig. 11.** Baryonic mass fraction at $z = 10$ per interval of the baryonic density contrast and per interval of the bulk temperature in the $S_{3T}$ simulation (*left panel*) and per interval of gas temperature in the $S_{1T}$ simulation (*right panel*), both simulations including photoionization processes.

not the aim of this paper, we do not give the details of the numerical aspects of this implementation (see Alimi & Courty, in preparation). Photo-ionization rates and heating rates are computed from the evolution of the hydrogen and helium densities and from the spectrum of the ultraviolet radiation background. Following Weinberg et al. (1997) the photoionizing background is assumed to have a redshift-dependent evolution, with the bulk of the transition between $z = 7$ and $z = 6$ and the peak between $z = 3$ and $z = 1$. Moreover, as shown in the numerical study by Gnedin (2000), we take into account a shallow evolution of the ultraviolet background intensity before $z \sim 7$ and begin the ionization processes at the redshift of 11.5. The radiation is considered as a spatially uniform field over the computational volume. We compute the baryonic mass fraction per interval of baryonic density contrast and per interval of temperature, which is the bulk temperature for the $S_{3T}$ simulation (Eq. (22)). Figure 11 shows that at $z = 10$ a fraction of the plasma is warmer in the simulation with non-equipartition processes than in the $S_{1T}$ simulation. At $z = 8$ no differences can be seen between the two simulations. This suggests that the IGM is warmer in a simulation with non-equipartition processes only before the universe has been completely reionized. However to draw any firm conclusions concerning the temperature differences between heavy particles and electrons before this epoch, simulations including a more careful treatment of how reionization proceeds should be performed, which is currently out of reach.

As mentioned above, non-equipartition requires structures such that cooling is dominated by atomic processes and the question is now to examine whether such structures exist at high redshift. Figure 12 illustrates the mass and the collapsing redshift of a $\nu$–$\sigma$ fluctuation computed in the top-hat collapse spherical model and with cosmological parameters of our $\Lambda$ cold dark matter model. Here, $\nu$ is the relative amplitude of fluctuation of scale $M$ in units of the filtered dispersion $\sigma(M, z = 0)$ at $z = 0$:

$$\nu = \frac{\delta_{\rm lin}^{\rm coll}}{\sigma(M, z = 0) D(z)}, \qquad (34)$$

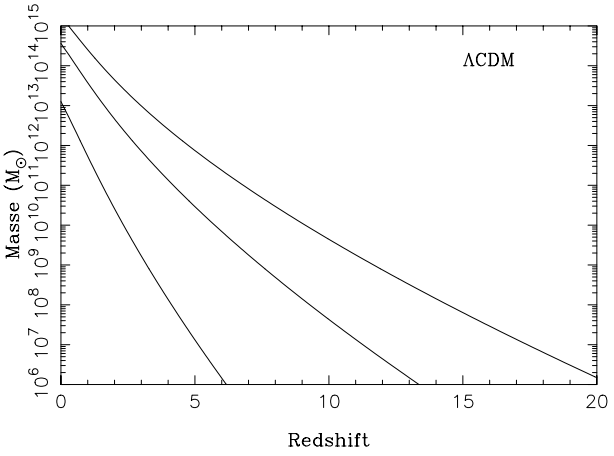


**Fig. 12.** Collapsing redshift and mass of (1–2–3)$\sigma$ fluctuations (from left to right), computed by a spherical top-hat collapse model (Eq. (34)) in a $\Lambda$-cold dark matter universe.

with $\delta_{\rm lin}^{\rm coll}$ the critical spherical overdensity at $z = 0$ and $D(z)$ the growth factor (Padmanabhan 1993). Before $z = 10$, which is likely before the end of the epoch of reionization, $3\sigma$ fluctuations have already collapsed. These curves are plotted in a simplified way and we refer to Hutchings et al. (2002) for recent studies. In a virialized approach, structures with mass higher than a minimal mass of around $10^8$ $M_\odot$ are known to cool efficiently by atomic processes and the so-called virialization temperature is larger than $10^4$ K. But as numerical simulations do not make any assumptions about the temperature of the IGM, we perform a high resolution simulation taking non-equipartition processes into account to check if structures with an out of equilibrium plasma are present at redshift higher than the epoch of reionization. The number of dark matter particles and grid cells is now equal to $384^3$ for the same computational box length, allowing the initial density fluctuation spectrum to include smaller scale modes.

This high resolution simulation is then able to catch bound structures at very high redshift. An example of such a structure at $z = 12$ is illustrated in Fig. 13 and temperature profiles along an horizontal line of sight through the structure is plotted

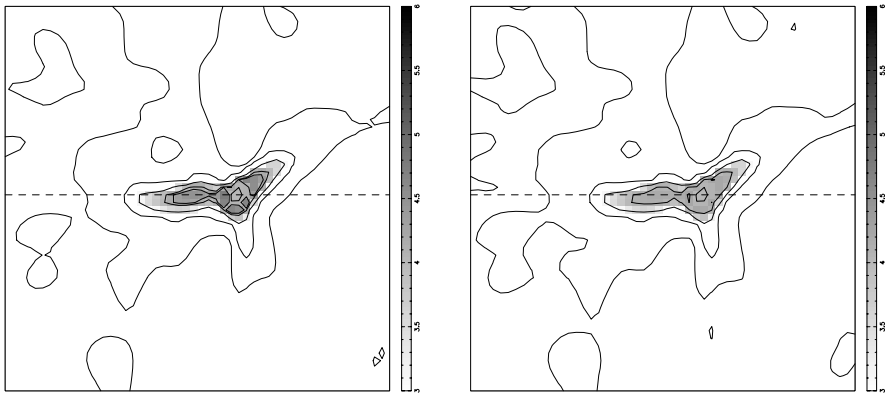

**Fig. 13.** Heavy particle (*left panel*) and electron (*right panel*) temperature distributions at $z = 12$ for the high resolution $S_{3T}$ simulation with $N_p = N_g = 384^3$ (the slices are 2.166 comoving $h^{-1}$ Mpc on a side and contour levels are: 2, 3, 10, $10^3$, $1.1\times10^4$, $1.7\times10^4$, $2.5\times10^4$, $2\times10^5$ K).

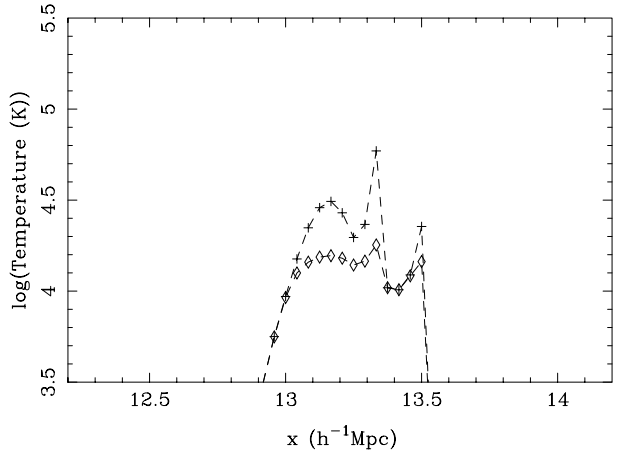


**Fig. 14.** Temperature profiles along a line of sight (dashed line in Fig. 13) in the structure at $z = 12$ for the high resolution $S_{3T}$ simulation: heavy particle temperature (plus sign), electron temperature (diamond sign).

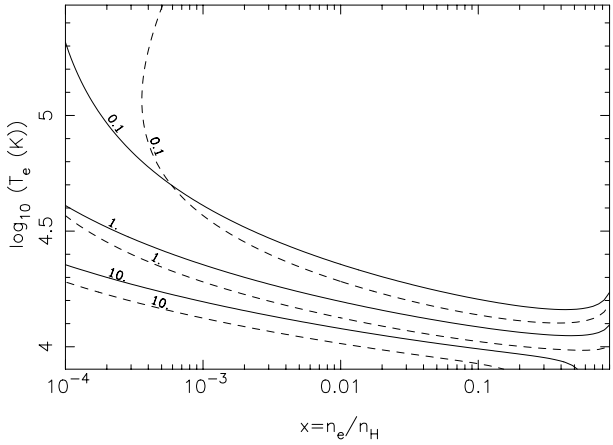


**Fig. 15.** Isocontours in a electron temperature-ionization degree diagram of cooling timescales computed with Eqs. (35) (dashed curves) and (36) (solid curves) normalized to the dynamical timescale (Eq. (37)), the labels on each curves are the ratios $t_{cool}/t_{dyn}$.

in Fig. 14. Similar differences between the electron and heavy particle temperatures can be seen in the outer regions of the structure as previously reported in the lower resolution simulation. It has to be mentioned that the computational size is $L = 16\ h^{-1}$ Mpc and that a lower box size would show a more resolved structure. We conclude that the introduction of non-equipartition processes leads to an out of equilibrium IGM, and that their influence is likely to be dominant at epochs before complete reionization of the universe. This plasma is involved in the galaxy formation process and we now turn to the cosmological implications.

### 5.2. On galaxy formation

Galaxy formation is closely related to the ability of gas to cool. One necessary condition for the collapse of gas clouds is that the cooling timescale must be less than the dynamical timescale. Cooling rates depend on the electron density and we have seen that, in out of equilibrium regions, the electron density can be lower by up to two orders of magnitude than in the simulation with equipartition processes forced. We compare the cooling timescales computed for an out of equilibrium plasma (subscript NE) and for a plasma in equilibrium (subscript E). In the first case the plasma temperature is the bulk temperature, mainly the heavy particle one:

$$(t_{cool})_{NE} = \frac{3/2kn_{tot}T_g}{Q_{cool}(T_e, x)}, \tag{35}$$

$$(t_{cool})_{E} = \frac{3/2kn_{tot}T}{Q_{cool}(T_e, x)}. \tag{36}$$

Note that in the second expression, the electron temperature in the cooling rate term is also the temperature of the plasma, $T = T_e$. These timescales are normalized to the dynamical timescale:

$$t_{dyn} = \sqrt{\frac{3\pi}{32G\rho}}, \tag{37}$$

and are plotted in Fig. 15 as a function of the ionization degree and the electron temperature, since this temperature controls the cooling rates. In these expressions $Q_{cool}$ is computed from Eq. (27), $n_{tot}$ is fixed at $5\times10^{-5}$ cm$^{-3}$, $n_H$ is given by $n_{tot}/(1+x)$ and $\rho$ is $n_H m_p + n_e m_e$. In Eq. (37) $\rho$ is multiplied by a factor of 10 to include the dark matter component.

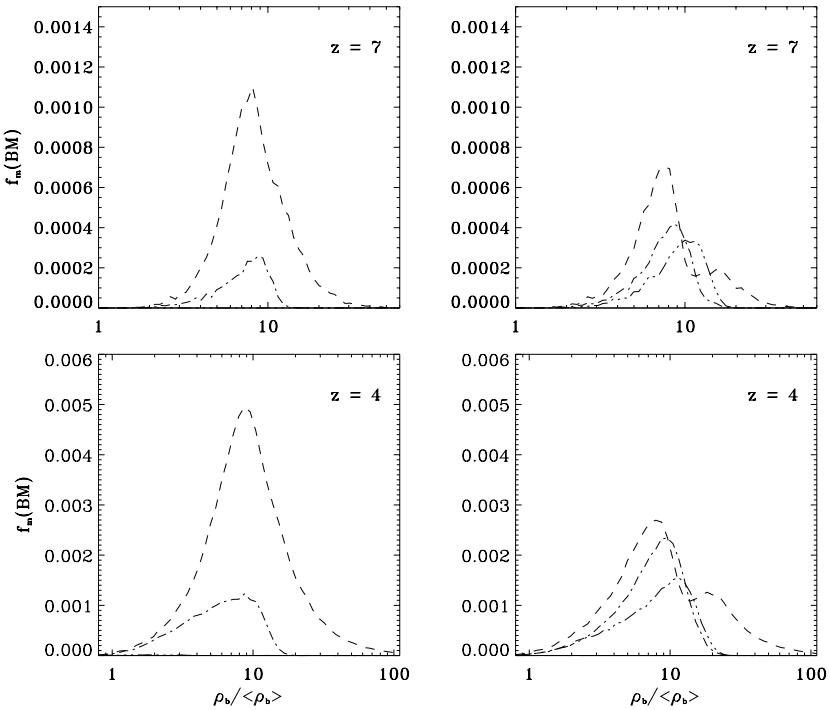


**Fig. 16.** Baryonic mass fraction per interval of the baryonic density contrast computed at two redshifts for different ranges of temperature: $8 \times 10^3 \leq T < 1.7 \times 10^4$ K (dashed line), $1.7 \times 10^4 \leq T < 3 \times 10^4$ K (dot-dashed line), $3 \times 10^4 \leq T < 5 \times 10^5$ K (triple dot-dashed line) in the $S_{3T}$ (*right panels*) and the $S_{1T}$ (*left panels*) simulations.

Two points matching the thermodynamical state of the plasma in the two simulations are worth mentioning. A point located at $x = 5 \times 10^{-4}$ and $T_e = 1.5 \times 10^4$ K mimics the warm weakly ionized baryonic matter in the outer regions of not too dense structures (such as in Fig. 2) seen in the $S_{3T}$ simulation. A point located at $x = 10^{-1}$ and $T_e = 2 \times 10^4$ K mimics the cold partially ionized baryonic matter in similar structures in the $S_{1T}$ simulation. Figure 15 shows that the first point is in the region $t_{cool} > t_{dyn}$ whereas the second point is in the region $t_{cool} < t_{dyn}$. This suggests that the out of equilibrium plasma in the $S_{3T}$ simulation is already cooled in the $S_{1T}$ simulation. Thus the cooling timescale is expected to be longer in simulations taking into-account non-equipartition processes.

We therefore estimate the cold baryonic mass fraction in the two simulations. Figure 16 presents the baryonic mass fractions computed at two redshifts as a function of the baryonic density contrast in three ranges of temperature: $8 \times 10^3 \leq T < 1.7 \times 10^4$ K, $1.7 \times 10^4 \leq T < 3 \times 10^4$ K and $3 \times 10^4 \leq T < 5 \times 10^5$ K. First of all we notice that the plots for the $S_{3T}$ simulation show a warm phase ($3 \times 10^4 \leq T < 5 \times 10^5$ K) which is not found in plots for the $S_{1T}$ simulation. As explained above, this phase in the $S_{3T}$ simulation is cold in the latter simulation and this is the second point to notice: the mass fraction of cold gas ($8 \times 10^3 \leq T < 1.7 \times 10^4$ K) is lower in the $S_{3T}$ simulation than in the $S_{1T}$ simulation. We have previously shown the evolution in redshift of the warm and cold fractions in Fig. 6. Since this cold phase is a reservoir for galaxy formation, this analysis of the thermodynamic properties and distributions of baryonic matter, strongly suggests that modifications in galaxy formation are to be expected in models with non-equipartition processes. This issue will be quantified in a forthcoming paper focusing on simulations including non-equipartition processes and galaxy formation (Alimi & Courty, in preparation).

## 6. Conclusions

We have considered in this paper the influence of non-equipartition processes on the thermodynamic properties of baryons in the universe, using numerical simulations of large scale structure formation. In the $S_{3T}$ simulation each species of the plasma, electrons, ions and neutral particles, has its own kinetic energy. The results have been compared with the $S_{1T}$ simulation in which equipartition processes are forced. In the $S_{3T}$ simulation, plasma is out of equilibrium in the outer regions of structures where the accreted baryonic matter is shocked or gravitationally compressed. The causes of the departure from equilibrium depend on the interaction mechanisms and thus on the thermodynamics of the accreted plasma. In the intra cluster medium of massive structures, baryons are shock heated to very high temperatures ($\sim 10^8$ K) and the equipartition timescale between ions and electrons is of the order of the Hubble time. But in low mass structures we have pointed out that departure from equilibrium in weakly ionized accreted plasma is driven by interactions between electrons and neutral particles. In that case the temperature differences are in the range $10^4$–$10^6$ K and in the $S_{3T}$ simulation the plasma is found to be warmer than in the $S_{1T}$ simulation. We have checked that the thermodynamic differences are not due to artificial heating. Since the energy exchange timescale between neutral particles and electrons is relatively short compared to the Hubble time, we have estimated semi-analytically the relaxation timescale in weakly ionized low temperature out of equilibrium regions. We have

shown that departure from equilibrium results from the competition between the cooling rates of the electrons and their heating rates by heavy particles. The relaxation timescale has been found to be long enough to yield departure from equilibrium. Moreover a semi-analytical relation between heavy particle and electron temperatures parameterized by the ionization degree has been derived and our numerical results are in a good agreement with this relation. Finally, we have discussed the cosmological implications of the warmer intergalactic medium in simulations taking non-equipartition processes into account: we have concluded that galaxy formation is expected to be modified and this issue will be studied in detail in forthcoming papers, in terms of galaxy properties and galaxy clustering.

*Acknowledgements.* Numerical simulations of this paper were performed on NEC-SX5 at the I.D.R.I.S. computing center (France). We thank Arturo Serna and Gunnlaugur Björnsson for a careful reading of the paper and the referee, Andrea Ferrara, for his constructive comments. J.M.A. thanks Laurent Moog (young student, now deceased) for fruitful discussions about the cosmological constant. S.C. acknowledges partial support from a special grant from the Icelandic Research Council during the final stages of this work.

## References

Bardeen, J., Bond, J., Kaiser, N., & Szalay, A. S. 1986, ApJ, 304, 15
Black, J. H. 1981, MNRAS, 197, 553
Bunn, E. F., & White, M. 1997, ApJ, 480, 6
Cen, R. 1992, ApJS, 78, 341
Cen, R., Gnedin, N. Y., & Ostriker, J. P. 1993, ApJ, 417, 387
Cen, R., & Ostriker, J. P. 1993, ApJ, 417, 404
Chièze, J.-P., Alimi, J.-M., & Teyssier, R. 1998, ApJ, 495, 630
Davé, R., Cen, R., Ostriker, J. P., et al. 2001, ApJ, 552, 473
Draine, B. T., & Katz, N. 1986, ApJ, 306, 655
Evrard, A. E., Summers, F. J., & Davis, M. 1994, ApJ, 422, 11
Fadeyev, Y. A., & Gillet, D. 1998, A&A, 333, 687
Fardal, M. A., Katz, N., Gardner, J. P., et al. 2001, ApJ, 562, 605
Fox, D. C., & Loeb, A. 1997, ApJ, 491, 459
Gnedin, N. Y. 2000, ApJ, 535, 530
Hutchings, R. M., Santoro, F., Thomas, P. A., & Couchman, H. M. P. 2002, MNRAS, 330, 927
Katz, N., & Gunn, J. E. 1991, ApJ, 377, 365
Katz, N., Keres, D., Dave, R., & Weinberg, D. H. 2002, [arXiv:astro-ph/0209279]
Kay, S. T., Pearce, F. R., Jenkins, A., et al. 2000, MNRAS, 316, 374
Padmanabhan, T. 1993, Structure formation in the Universe (Cambridge: University Press)
Petschek, H., & Byron, S. 1957, Ann. Phys., 1, 270
Rees, M. J., & Ostriker, J. P. 1977, MNRAS, 179, 541
Shchekinov, I. 1991, Ap&SS, 175, 57
Silk, J. 1977, ApJ, 211, 638
Spitzer, L. 1962, Physics of fully ionized gases, 2d ed. (New York: Interscience)
Sugiyama, N. 1995, ApJS, 100, 281
Sunyaev, R. A., & Zel'dovich, Y. B. 1972, A&A, 20, 189
Takizawa, M. 1998, ApJ, 509, 579
Takizawa, M., & Mineshige, S. 1998, ApJ, 499, 82
Teyssier, R., Chièze, J.-P., & Alimi, J.-M. 1998, ApJ, 509, 62
Von Neumann, J., & Richtmyer, R. 1950, J. Appl. Phys., 21, 232
Weinberg, D. H., Hernquist, L., & Katz, N. 1997, ApJ, 477, 8
White, S. D. M., & Rees, M. J. 1978, MNRAS, 183, 341
Zel'dovich, Y. B., & Raizer, Y. P. 1966, Physics of shock waves and high-temperature hydrodynamic phenomena (New York: Academic Press)